The LINNEAN SOCIETY of London BOTANICAL Journal of the Linnean Society

*Botanical Journal of the Linnean Society*, 2014, **175**, 423–437. With 6 figures

# The earliest wood and its hydraulic properties documented in *c.* 407-million-year-old fossils using synchrotron microtomography

CHRISTINE STRULLU-DERRIEN[1,2]*, PAUL KENRICK[1], PAUL TAFFOREAU[3], HERVÉ COCHARD[4,5], JEAN-LOUIS BONNEMAIN[6], ALAIN LE HÉRISSÉ[7], HUBERT LARDEUX[8] and ERIC BADEL[4,5]

[1]*Department of Earth Sciences, The Natural History Museum, Cromwell Road, London SW7 5BD, UK*
[2]*Laboratoire Mycorhizes, Faculté des Sciences, Université d'Angers, 2 boulevard Lavoisier, 49045 Angers cedex, France*
[3]*European Synchrotron Radiation Facility, 6 rue Jules Horowitz, 38043 Grenoble cedex, France*
[4]*INRA, UMR547 PIAF, 63100 Clermont-Ferrand, France*
[5]*Université Blaise Pascal, UMR547 PIAF, Clermont Université, 63000 Clermont-Ferrand, France*
[6]*Laboratoire Ecologie et Biologie des Interactions, UMR CNRS 7267, Université de Poitiers, 40 avenue du Recteur Pineau, 86022 Poitiers cedex, France*
[7]*UMR 6538 Domaines Océaniques, CNRS, IUEM, Université de Brest, 6 avenue Le Gorgeu, CS 93837, 29238 Brest cedex 3, France*
[8]*Le Verger-Beaucé, 35520 Melesse, France*

*Received 20 July 2013; revised 28 March 2014; accepted for publication 11 April 2014*

We document xylem structure and hydraulic properties in the earliest woody plant ***Armoricaphyton chateaupannense* gen. nov. & sp. nov.** based on *c.* 407-million-year-old fossils from the Armorican Massif, western France. The plant was small, and the woody axes were narrow and permineralized in pyrite ($FeS_2$). We used standard palaeobotanical methods and employed propagation phase contrast X-ray synchrotron microtomography (PPC-SRμCT) to create three-dimensional images of the wood and to evaluate its properties. The xylem comprised tracheids and rays, which developed from a cambium. Tracheids possessed an early extinct type of scalariform bordered pitting known as P-type. Our observations indicate that wood evolved initially in plants of small stature that were members of Euphyllophytina, a clade that includes living seed plants, horsetails and ferns. Hydraulic properties were calculated from measurements taken from the PPC-SRμCT images. The specific hydraulic conductivity of the xylem area was calculated as 8.7 kg $m^{-1}$ $s^{-1}$ and the mean cell thickness-to-span ratio $(t/b)^2$ of tracheids was 0.0372. The results show that the wood was suited to high conductive performance with low mechanical resistance to hydraulic tension. We argue that axis rigidity in the earliest woody plants initially evolved through the development of low-density woods.  *Botanical Journal of the Linnean Society*, 2014, **175**, 423–437.

ADDITIONAL KEYWORDS: *Armoricaphyton chateaupannense* – Devonian – hydraulic conductivity – pyrite – tracheids – wood.

*Corresponding author. E-mail: c.strullu-derrien@nhm.ac.uk

## INTRODUCTION

Forests first appeared on land during the mid-Devonian (393–383 Ma), and evidence from fossils shows that trees evolved in several groups of vascular plants independently and that diverse strategies were employed (Niklas, 2000; Meyer-Berthaud, Soria & Decombeix, 2010). One of the key developments was the acquisition of wood, which evolved independently in two clades (lycophytes, euphyllophytes) (Kenrick & Crane, 1997a, b) and possibly several more (Boyce, 2010). Detailed descriptions of early fossil woods indicate that the initial assembly of this tissue system involved the piecemeal acquisition of various developmental features and therefore elements of functionality (Donoghue, 2005; Pittermann, 2010; Spicer & Groover, 2010). At the cellular level, a progressive increase in tracheid lumen diameter coincided with the evolution of large plants, and this is thought to have enhanced fluid conductance (Niklas, 1985; Pittermann, 2010), but the unique features of the secondary wall of early tracheids (Kenrick & Crane, 1991, 1997a,b; Edwards, 2003; Edwards, Li & Raven, 2006) complicate the analysis of hydraulic function (Sperry, 2003; Pittermann, 2010; Wilson & Fischer, 2011). Understanding the evolution of wood requires a detailed documentation of early fossil materials, knowledge of their phylogenetic context and a critical analysis of their functional properties. Here, we document the wood anatomy of *Armoricaphyton chateaupannense* gen. nov. & sp. nov. from the Lower Devonian Chalonnes Formation of the Anjou area (Armorican Massif) of western France (*c.* 407 Ma; Strullu-Derrien, 2010; Strullu-Derrien *et al.*, 2010; Gerrienne *et al.*, 2011). The plant was small with narrow axes (1.5–2.5 mm wide), and its wood was permineralized in pyrite ($FeS_2$). We used standard palaeobotanical methods and employed propagation phase contrast X-ray synchrotron microtomography (PPC-SRμCT) to create detailed submicrometre-scale, three-dimensional images that enabled virtual dissection of the wood and the characterization of its properties. Hydraulic and biomechanical properties were calculated from measurements derived from the PPC-SRμCT images. Several types of fossil plants and plant organs have been documented using X-ray computed tomography (also called microtomography or micro-CT) (e.g. DeVore *et al.*, 2006; Collinson *et al.*, 2012; Gee, 2013) and high-resolution X-ray synchrotron microtomography (PPC-SRμCT) (e.g. Feist, Liu & Tafforeau, 2005; Friis *et al.*, 2007; Smith *et al.*, 2009; Collinson *et al.*, 2013; Friis, Pedersen & Endress, 2013). These techniques have also been used for the study of wood structure in extant plants (e.g. Mannes *et al.*, 2010; Brodersen *et al.*, 2011). We show that PPC-SRμCT is a valuable new method for the characterization of the anatomy and hydraulics of early fossil woods.

## MATERIAL AND METHODS

### Geological context

The Armorican Massif represents the western part of the Late Palaeozoic Variscan Belt that extended throughout western and central Europe (Fig. 1A). During the Early Devonian, the Armorican Massif comprised an assemblage of terranes, including land and shallow-shelf siliciclastic platforms that alternated with carbonate platforms. Palaeogeographically, this region was located on or close to the northern margin of Gondwana (Morzadec *et al.*, 1988) (Fig. 1D). The southern part of this massif includes the Chateaupanne Unit, which comprises two Early Devonian plant-bearing levels (Fig. 1C). The first of these outcrops occurs in several quarries located south of the Loire River; the second, corresponding to the Basal Member of the Chalonnes Formation, outcrops only in the Châteaupanne Quarry (Montjean-sur-Loire, Maine et Loire) (Fig. 1B). Fourteen outcrops containing plants have been reported from this quarry since the first discovery by H. Lardeux in 1969. Only seven outcrops are still accessible, and the specimens described here were collected from two of them. The geology, sedimentology and palynology of the Basal Member of the Chalonnes Formation were described in detail by Strullu-Derrien *et al.* (2010). The age of the plant-bearing horizon was determined as late Pragian to earliest Emsian (*c.* 407 Ma) based on palynological analyses (Strullu-Derrien *et al.*, 2010; Gerrienne *et al.*, 2011).

### Photographic, microscopic and microtomographic analyses

The description is based on axes showing two types of preservation: (1) adpressions (i.e. axes preserved as a combination of impression and thin coaly compression); and (2) permineralizations or partial permineralizations in pyrite ($FeS_2$). Twenty samples were studied: five blocks of rock containing numerous plants and 15 individual plant axes. Permineralizations were detected within the shale matrix using a Faxitron X-ray system equipped with a Faxitron camera (Edimex, Angers, France) (setting: 30 kV, 0.30 mA; exposure 20 s) (Fig. 2A). Once the positions were located, the blocks were trimmed using a diamond blade saw, embedded in polyester (GTS) resin and sectioned to a thickness of approximately 1.5 mm, following the methods outlined in Jones & Rowe (1999). These sections were mounted on glass slides using epoxy resin and ground mechanically to create a flat surface for examination and photography.

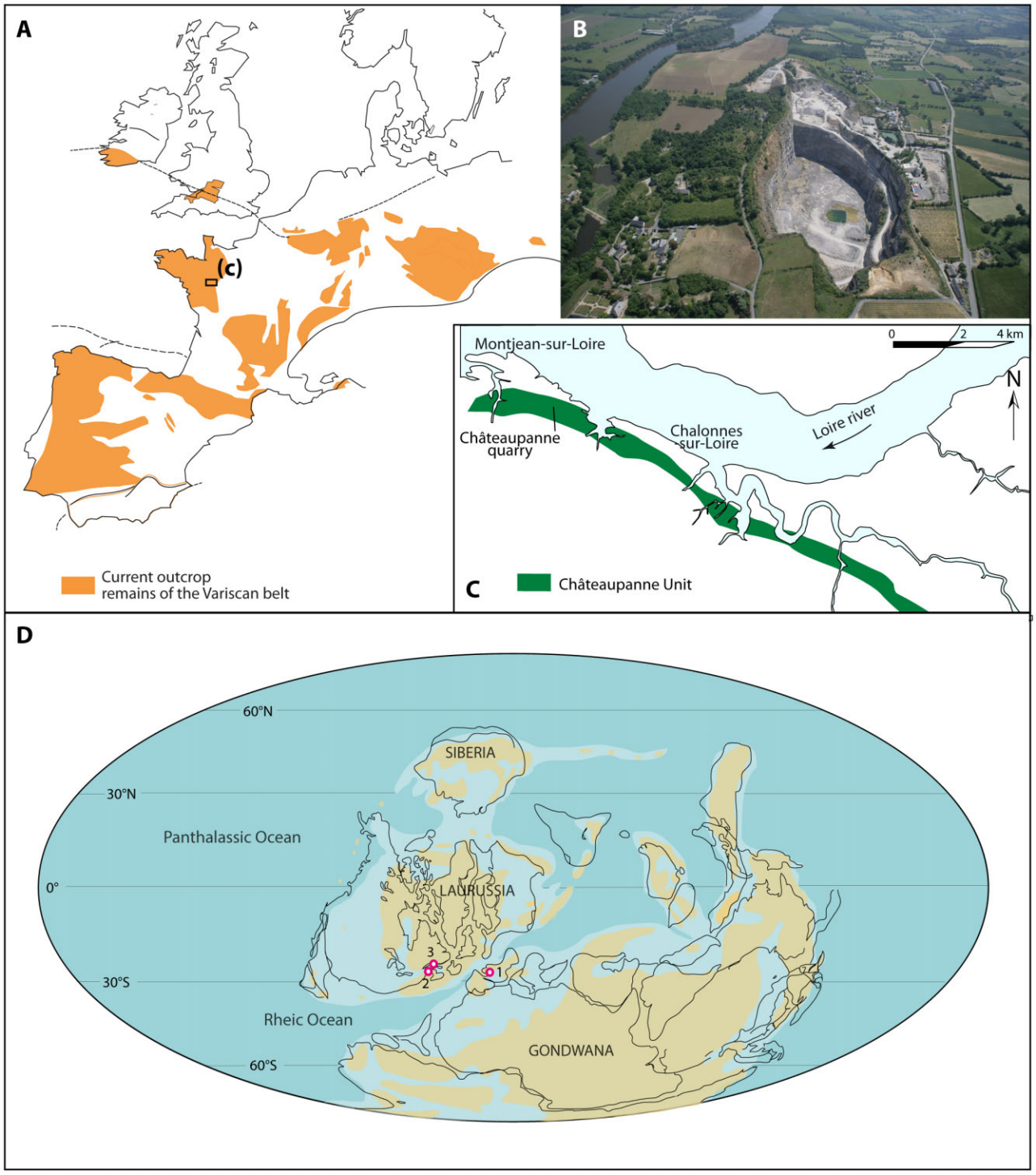


**Figure 1.** Location of the study area and palaeogeography. A, Location [rectangle expanded in (C)] of the study area in the European Variscan Belt and the Armorican Massif. B, The Châteaupanne Quarry (aerial view) with permission of R. Jospin. C, Lower Devonian deposits from the Anjou area (Châteaupanne Unit). D, Early Devonian palaeogeography (after Scotese, 2001, modified). Continental land masses are indicated in light brown and shelves in light blue; the fine line drawing indicates the outlines of the present continents. Geographical relationships of the sites of the three early woody plants: 1, Anjou area in the Armorican Massif (western France); 2, New Brunswick, Canada; 3, Gaspé, Canada.

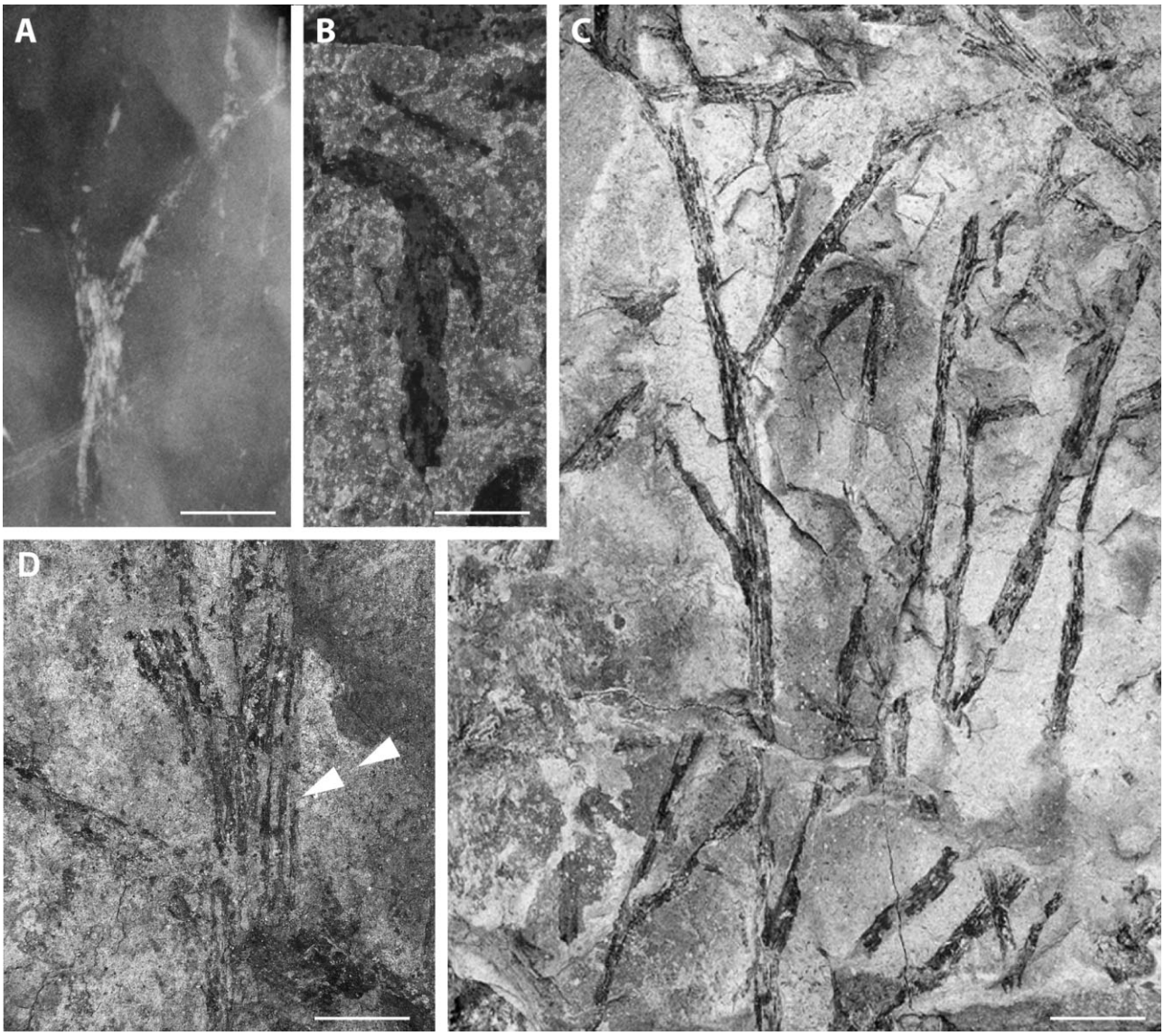


**Figure 2.** Morphology of the axes. Specimen CSD-06M-02: paratype. A, Faxitron X-ray system image of a permineralized specimen embedded within the shale matrix showing the arrangement of the axes (Specimen CSD-06M-02). B, Pair of fusiform sporangia twisted around each other (Specimen CSD-06M-03B). C, Axes in compression bifurcating to produce helically arranged lateral branches (Specimen CSD-07M-01). D, Higher magnification of (C). Axes bear longitudinal ribs (arrows) (Specimen CSD-07M-01). Scale bars: 3 mm (A, D); 2 mm (B); 4.5 mm (C).

Ground sections were etched briefly with nitric acid following the method described in Kenrick (1999). The etched specimens were photographed using a Zeiss photomicroscope with a polarized light source. Several samples were selected for scanning electron microscopy. Some specimens were gold coated and examined using a JSM5800 at 5 keV (Université de Liège, Belgium). Others were carbon coated and examined using a JSM6301F at 5–30 keV (Université d'Angers, France).

To study the three-dimensional structure of the pyritized wood non-destructively, we undertook a microtomographic analysis using the tomography beamline ID19 of the European Synchrotron Radiation Facility (ESRF), Grenoble, France (Feist *et al.*, 2005). A specimen was prepared by embedding in resin and sectioning following the method outlined above. A small block was cut (10 mm × 8 mm × 3 mm), which comprised a short length of pyritized axis with attached shale and embedding resin.

Because the volume of interest (pyritized specimen within our cut block) was larger than the field of view of 2 mm and quite dense, we used an approach based on local tomography employing a beam set at 30 keV with a multilayer monochromator. A detector based on a GGG:Eu (Gadolinium Gallium Garnet) single crystal scintillator (thickness, 10 μm) with a microscope system, coupled to a CCD FReLoN camera (Fast Readout Low Noise), was employed to obtain an isotropic voxel size of 0.551 μm. To reveal the finest details, we used a propagation distance of 20 mm between the sample and the detector, allowing moderate phase contrast effect. Because the sample was larger than the field of view, a half-acquisition approach (off axis centre of rotation) was applied to increase the field of view laterally, using 4000 projections of 1.2 s each over 360° and continuous rotation mode to improve results of local tomography (Lak *et al*., 2008). The volume reconstruction was performed using PyHST software (developed at ESRF).

In X-ray computed tomography, imaging is based on the attenuation of X-rays as they pass through the object, which is related to density and chemical composition. In our permineralized fossil, this is provided by the partitioning in the tracheid cell walls and lumens of the comparatively low average atomic weight organics (mainly $^{12}C$) from the comparatively high average atomic weight pyrite ($^{56}Fe$, $^{32}S$). This occurs in a consistent manner, so that the form and arrangement of cells can be clearly discerned. The volume was virtually segmented using VGStudioMax 2.0 (Volume Graphics, Heidelberg, Germany) to remove the pyrite and generate the three-dimensional renderings and the virtual thick three-dimensional histological sections, following protocols adapted from dental palaeohistology (Tafforeau & Smith, 2008). The effect achieved is similar to that of a deep acid etch, in which the pyrite is removed chemically (e.g. Kenrick, 1999). The method enables virtual sectioning of the wood and the tracheid cell walls to a maximum voxel size, in this instance of 0.551 μm. This level of resolution is sufficient to characterize the general structure and hydraulic properties of the wood.

## Calculations of hydraulic properties

For hydraulic conductivity properties, we applied a typical model of hydraulic resistance in long conduits (Tyree & Zimmermann, 2002). We assumed that the tracheids are axial conduits having a constant section. For a laminar flow under a uniform pressure gradient along the $z$ direction, the Poisson equation can be written as follows:

$$\nabla^2 u = \frac{1}{\mu}\frac{\mathrm{d}P}{\mathrm{d}z} \tag{1}$$

The flux $q$ in the conduit can be written as:

$$q = -k\frac{\mathrm{d}P}{\mathrm{d}z} \tag{2}$$

where $k$ is the hydraulic conductivity, $u$ is the fluid speed in the conduit, $\mu$ is the viscosity of the fluid and $P$ is the pressure. This Poisson equation and the hydraulic conductivity thereby expressed can only be solved exactly for simple shapes, such as discs, rectangles, etc. In the case of a perfect circular cylinder, the conductivity of the conduit varies with the diameter to the power of four. In the case of non-simple shapes, several methods are available that allow the conductivity to be approximated. We refer the reader to the paper of Sisavath, Jing & Zimmerman (2001) for a comparison of these methods. In our work, the individual conductivities $k_i$ of the cells were computed using the hydraulic diameter approximation proposed by Sisavath *et al*. (2001) for undefined cross-sections of conduits:

$$k_i = \frac{1}{32}\mu {D_{\mathrm{H}i}}^2 A_i \tag{3}$$

where $A_i$ is the cross-sectional area of the conduit and $D_{\mathrm{H}i}$ is its hydraulic diameter, defined as the area to perimeter ($p_i$) ratio:

$$D_{Hi} = \frac{4A_i}{p_i} \tag{4}$$

The total conductivity $k_{\mathrm{Tot}}$ of the system is the sum of the individual conductivities of each cell:

$$k_{\mathrm{Tot}} = \sum k_i \tag{5}$$

Shape parameters ($A_i$ and $p_i$) of cell lumens were measured on a transverse slice extracted from the PPC-SRμCT volume using ImageJ software (Rasband, 2012). A few poorly visible cell lumens were removed from the computation. Suitable cells were grouped into five clusters called regions of interest (ROIs). The total area $A_{xyl}$ of these ROIs, which represent the xylem that contains the cells, was measured. Finally, the specific conductivity $k_{\mathrm{s}}$ was computed as the sum of the individual conductivities $k_i$ divided by the total xylem area:

$$k_{\mathrm{S}} = \frac{\sum k_i}{A_{xyl}} \tag{6}$$

Hydraulic conductivity reflects the ability of the system to conduct a large volume of water. However, this performance is limited by other considerations, such as the risk of implosion. The larger the tracheid lumen and the thinner the cell walls, the more susceptible is the tracheid to mechanical buckling when high negative pressure occurs. This susceptibility can

be evaluated by the thickness-to-span ratio $(t/b)^2$, also called the 'implosion safety factor', where $b$ is the diameter of the cell and $t$ is the cell wall thickness. The complete mapping of the cell wall thickness was computed by image analysis using the Hildebrand algorithm (Hildebrand & Rüegsegger, 1996) and the implosion safety factor was evaluated.

## RESULTS

### Description of specimens

The description is based on fossilized axes of two types: adpressions and permineralizations. We describe each type separately, because, although closely associated at the site and of similar general form, they are not in organic connection. Our taxonomic description is based on the permineralized materials.

*Adpressions*

Adpressions preserve axes and sporangia as a combination of impression and thin coaly compression. Axes are up to 15 cm long, and range in width from 1.0 to 2.5 mm for the main axes, and from 0.8 to 1.5 mm for the first-order axes. Main axes divide anisotomously to produce lateral branches at intervals of approximately 15 mm. Angular divergence of first-order lateral branches is 120° (Fig. 2C). The axes exhibit conspicuous longitudinal ribbing (Fig. 2D), which may be the surface expression of underlying anatomical features (e.g. lignified sterome). Because both the sterome layer and the tracheids show the same type of preservation in our samples, we hypothesize that the cell walls in both were lignified. Isolated sporangia were found associated with the axis, and these may be part of the same plant. Sporangia are borne terminally in pairs, and are fusiform (6 mm long) with a distinctive helical twisting (Fig. 2B). The mode of dehiscence is unknown. These remains represent the distal portions of a larger plant, but the basal regions are not preserved.

*Permineralizations*

The cellular details of the vascular system are preserved in partially permineralized axial sections. The division of the main axis and ribbing is visible in the X-ray image (Fig. 2A). In transverse section, axes show a circular to elongate centrach primary xylem (Fig. 3A, B). External to the metaxylem, which shows no obvious alignment (Fig. 3B), most specimens show rows of ten radially aligned tracheids (Figs 3B, C, 4B, C). This number can reach 15 in some specimens. These aligned tracheids occupy a much greater proportion of the vascular cylinder (four-fifths) in larger axes (Fig. 3C). In transverse section, the tracheids are faceted (generally four sides) (Fig. 4B, C). The tracheid radial diameter is 15–100 μm; the tangential diameter is 15–70 μm. At several places, two radial files emanate from a single radial file of cells (Fig. 4B, C). Structures that we interpreted as rays are particularly clearly visualized in the PPC-SRμCT images (Fig. 4C, D). The capacity for virtual sectioning enables them to be traced within the aligned xylem (Fig. 4C, E). These rays and their spatial distribution were illustrated in Gerrienne *et al*. (2011: figs 1A, F, G, S2, S3, Supporting online material). The rays are rare, and their form and size are variable. We conclude from the evidence of rays and radially aligned tracheids, which are the product of periclinal division and correspond to the secondary xylem, that the plant possessed a vascular cambium. Evidence in favour of a cambium is also provided by the presence of anticlinal divisions in the wood, a feature also seen in cambium-derived wood of cladoxylopsids (Meyer-Berthaud *et al*., 2004), progymnosperms (Dannenhoffer & Bonamo, 2003) and extant woody plants (Lachaud, Catesson & Bonnemain, 1999; Pallardy, 2008). Poor preservation outside the central woody cylinder precludes the preservation of phloem. In a few axes in which the secondary xylem is not well developed, a layer of large thick-walled cells has been observed in the outer cortex (Fig. 3A). This layer is the partially preserved remains of a sterome which is one cell thick. A sterome located in the outer cortex is common in early land plants and is generally not observed in living plants. When the secondary xylem is well developed, tracheids with small radial diameters (arranged in a discontinuous layer) can sometimes be seen within this tissue. They are separated from the outer margin of the preserved secondary xylem by one (Fig. 3C, arrows), two or three (Gerrienne *et al*., 2011: figs 1 and S1, Supporting online material) tracheids with a larger radial dimension. This configuration of cells could indicate the presence of an incomplete growth layer boundary within the wood near its circumference or, perhaps, differences in the pattern of divisions of the fusiform initials along the cambial layer.

The wood is composed of numerous tracheids, and the cell wall structure is P-type (*sensu* Kenrick & Crane, 1997a,b), meaning that the cells possess scalariform bordered pits and a characteristic perforated sheet of secondary wall material that overlies the pit apertures (Figs 3D–F, 4E, 5). Images in scanning electron microscopy of fractured surfaces of pyritized cells are more difficult to interpret than virtual X-ray sections because there is less control over the plane of orientation. Pyrite crystals within the lumen and wall also obscure details of the coalified remains of the cell wall. However, using this method higher spatial resolution is achievable.

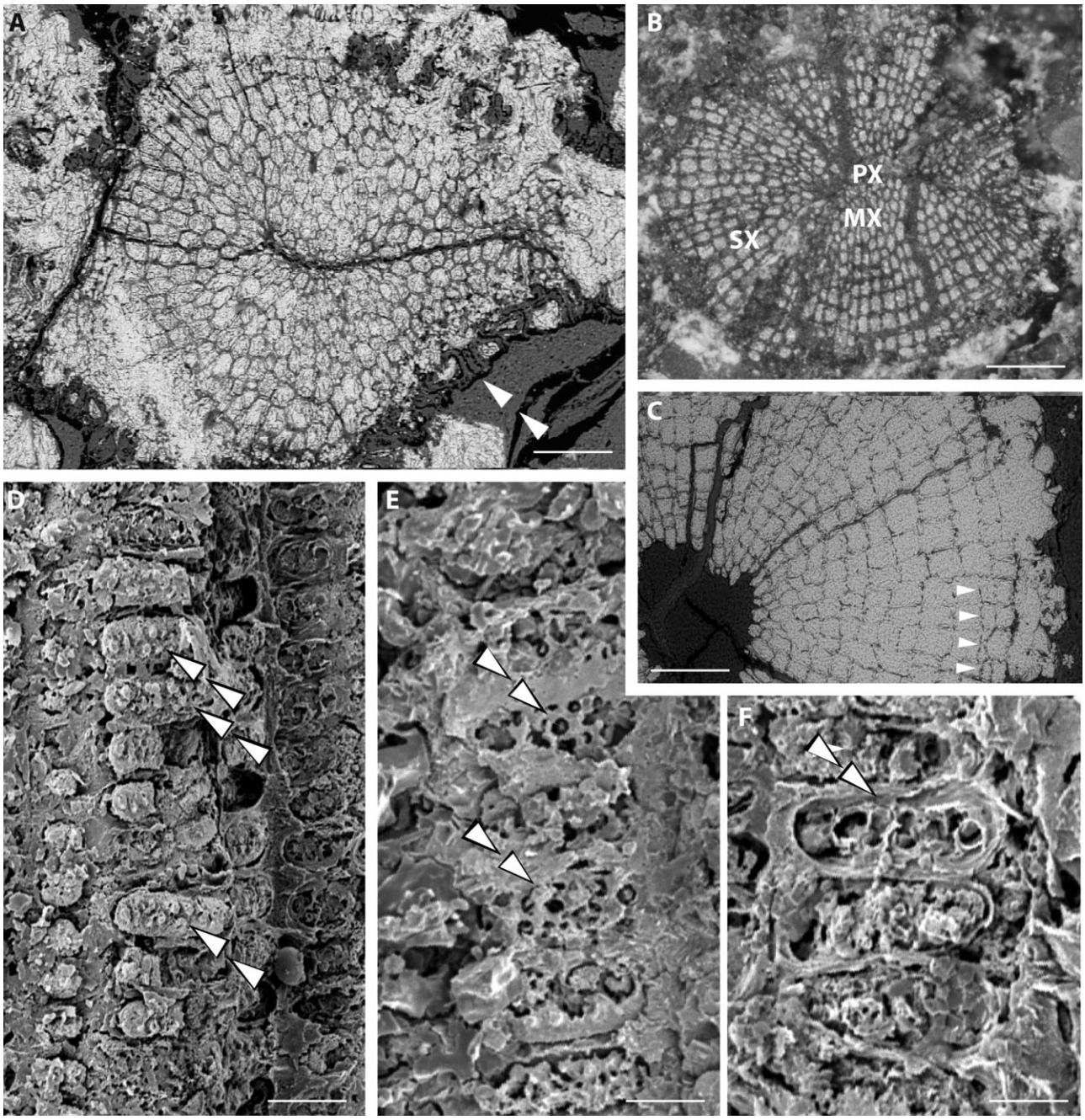


**Figure 3.** Anatomy of the axes. Specimens CSD-06C-04, CSD-06A-01: paratypes. A–C, Transverse sections of pyritized axes. A, Axis in which the secondary xylem is not well developed. A layer of large thick-walled cells (sterome) is visible in the outer cortex (arrows) [scanning electron microscopy (SEM), backscatter electrons] (Specimen CSD-06C-04). B, Axis showing both primary and secondary xylem; MX, metaxylem; PX, protoxylem; SX, secondary xylem (microscopy using polarized light source) (Specimen CSD-06A-01). C, Axis showing a primary xylem area (not preserved) surrounded by rows of ten radially aligned tracheids of secondary xylem. Some tracheids have a smaller radial diameter in places within the wood (arrows) (SEM, backscatter electrons) (Specimen CSD-06C-02). D–F, P-type tracheids fractured in longitudinal section to show aspects of the cell wall in different planes of fracture (SEM) (Specimen CSD-06A-01). D, Pyritized casts of the interior chambers of the scalariform bordered pits (arrows). E, Coalified remains of pit-closing perforated sheet in two partly visible pit fields (arrows). F, Row of scalariform bordered pits. The pit chamber cast has fallen out of one to reveal organic remains of the pit borders and part of the pit-closing perforated sheet (arrow). Scale bars: 200 μm (A, C); 300 μm (B); 14 μm (D, E); 7 μm (F).

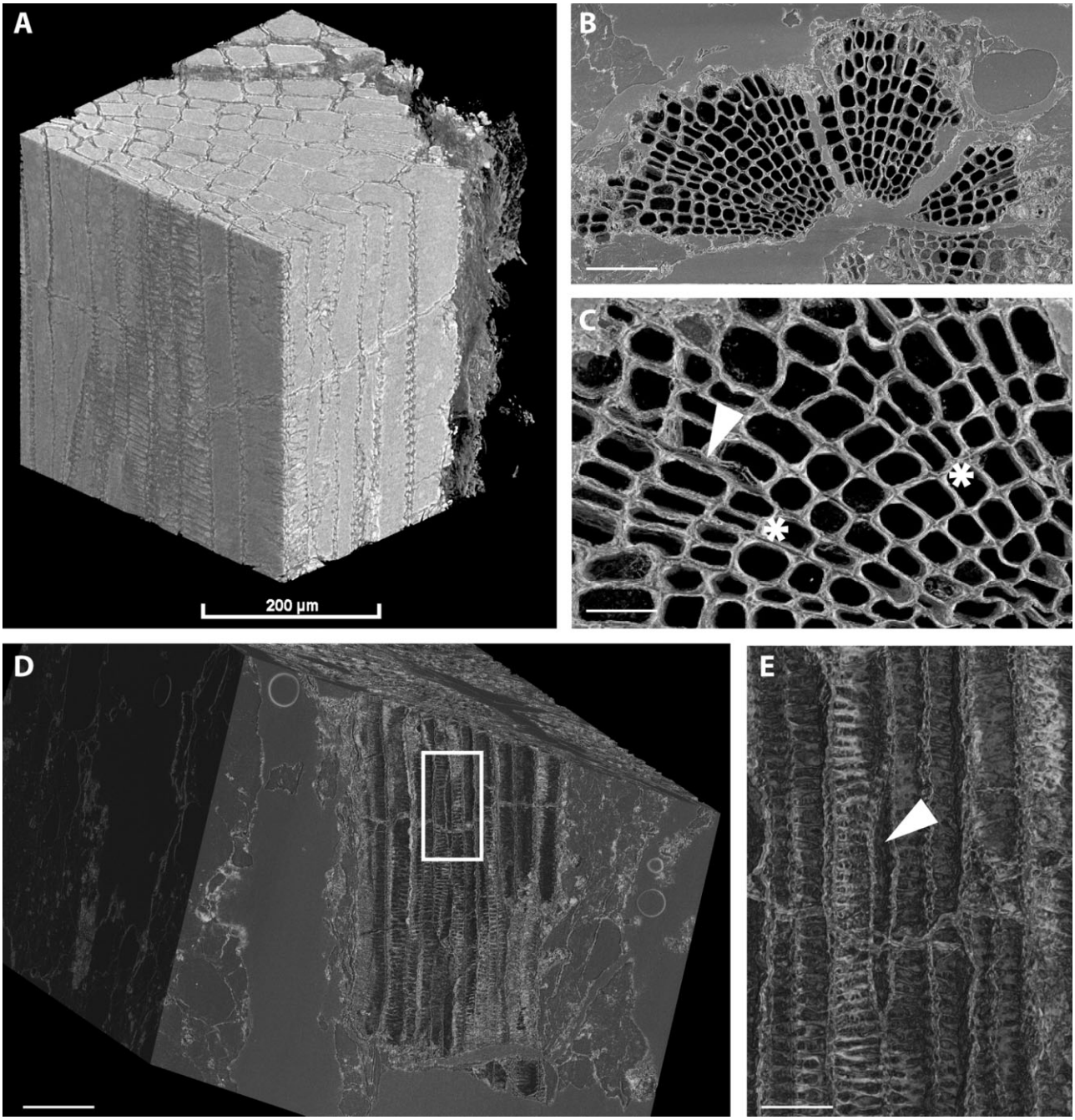


**Figure 4.** *Armoricaphyton chateaupannense*. Specimen CSD-07F-01: holotype. High-resolution propagation phase contrast X-ray synchrotron microtomography (PPC-SRµCT) of *c*. 407-million-year-old fossil wood preserved in the mineral pyrite ($FeS_2$). A, Three-dimensional representation of part of the pyritized axis, which has been virtually trimmed to a cubic volume. Xylem tracheids are visible in longitudinal, radial and transverse sections. B, Transverse section of part of the xylem embedded in a shale matrix. In this image, the mineral pyrite has been virtually dissected out, leaving behind the organic framework of the tracheid cell walls. C, Higher magnification of (B). Tracheids are generally rectangular in transverse section. In several places, two xylem cell rows emanate from a single row (asterisks); single-walled space interpreted as ray (arrow). D, Longitudinal tangential section of part of the xylem in which the pyrite has been virtually dissected. E, Detail of the framed area from (D); secondary xylem showing tracheids and a one-cell ray. A double wall (consisting of the secondary walls of each tracheid) is visible between adjacent tracheids, whereas a single wall occurs between ray (arrow) and tracheid cells. The wall of the ray was not preserved. Scale bars: 300 µm (B); 50 µm (C, E); 150 µm (D).

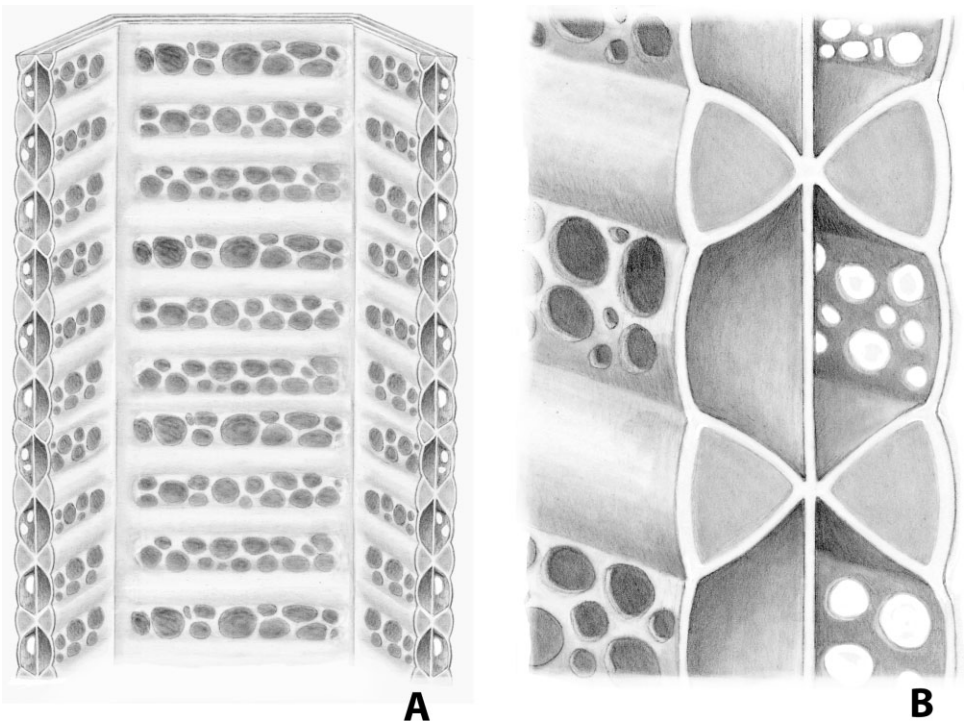


**Figure 5.** P-type tracheid. A, Reconstruction of a tracheid. Drawing of cut-away longitudinal section, showing interior of cell (×800). Cell with scalariform bordered pits with overarching pit borders and a characteristic perforated sheet of secondary wall material that overlies the pit apertures. B, Detail of tracheid cell wall construction (×2500). The cell wall comprises an inner layer facing the cell lumen, pit chambers, and an inner layer within the scalariform bars. The scalariform pit apertures are covered with a perforated sheet. Drawing by Pollyanna von Knorring, modified after Kenrick & Crane (1997a).

## SYSTEMATICS

*Euphyllophytina Kenrick & Crane (1997a)*

*Class incertae sedis*

Armoricaphyton *Strullu-Derrien gen. nov.*
*Diagnosis:* Plant with leafless axes that bifurcate pseudomonopodially to give first-order laterals. Axes bear longitudinal ribs. Xylem cylinder circular, comprising centrarch primary xylem and peripheral secondary xylem. Rays present. Tracheids with scalariform bordered pits with overlay of an additional perforate sheet of secondary wall material (P-type tracheid). Single outer cortical layer comprising thick-walled cells.

*Etymology:* From the Armorican Massif (western France).

*Armoricaphyton chateaupannense Strullu-Derrien, sp. nov.*
*Diagnosis:* As in generic diagnosis. Axis 1.5–2.5 mm wide and at least 12 cm long.

*Etymology:* From Latin '-ense', denoting the place (Châteaupanne Quarry, Montjean-sur-Loire, west of France) where the species was discovered.

*Holotype designated here:* pyritized axis = specimen CSD-07F-01 (Fig. 4A).

*Paratypes designated here:* pyritized axes = specimen CSD-06 M-02 (Fig. 2A); specimen CSD-06C-04 (Fig. 3A); specimen CSD-06A-01 (Fig. 3B, D, F). The materials are deposited in the Muséum d'Histoire naturelle, Angers (France), under the numbers: CSD-07F-01, CSD-06M-02, CSD-07M-01, CSD-06A-01, CSD-06C-02, CSD-06C 04, CSD-06M-03B.

*Locality:* Châteaupanne Quarry, Montjean-sur-Loire, Maine-et-Loire, France.

*Horizon:* Basal Member of the Chalonnes Formation, latest Pragian–earliest Emsian (Early Devonian, *c.* 407 Ma).

These samples are conspecific with those described in Gerrienne *et al.* (2011).

*Basis of taxonomic concept and other notes*

There is no direct evidence of connection between adpressions and permineralizations, and so we have based our taxonomic description on the permineralized specimens. However, we considered that the two types of material are probably conspecific based on strong corroboration from several lines of evidence. All the samples were collected from the same site and the same sedimentary layer. Both adpressions and permineralizations share some key features of morphology (Fig. 2A, C, D, E): they are of the same size and shape, and show the same type of branching. When cut transversally, the pyritized sample in the X-ray image (Fig. 2A) shows the same anatomy as other isolated pyritized axes located within the sediment. All the axes show the same form of external ribbing.

*Comparison between Armoricaphyton and the other Lower Devonian plants*

Anatomically, there are similarities between *Armoricaphyton* and *Psilophyton* Daws. (Gerrienne, 1997) in the form of the primary xylem and in the structure of the tracheid cell wall (Banks, Leclercq & Hueber, 1975; Hartman & Banks, 1980). *Armoricaphyton* differs from *Psilophyton* in the presence of secondary xylem with rays. Some minor radial alignment of xylem has been observed in the larger stems of *Psilophyton dawsonii* Banks, Leclercq & Hueber and in *Psilophyton crenulatum* Doran (Doran, 1980), but there is no evidence of rays or anticlinal divisions. Additional differences to *Psilophyton* in *Armoricaphyton* include a much narrower primary xylem cylinder and a sterome limited to one cell in thickness. No *Psilophyton* spp. have been observed associated with *Armoricaphyton*. Two other early Devonian woody plants have been reported to date: *Franhueberia gerriennei* (Hoffman & Tomescu, 2013) from Gaspé (Canada) and a plant that has not yet received a taxonomic assignation from New Brunswick (Canada) (Gerrienne *et al*., 2011: fig. 1D). These plants are derived from sediments of late Emsian age and are therefore slightly younger than *Armoricaphyton*. *Armoricaphyton* shares some resemblance with *Franhueberia gerriennei*, but distortion of the axis in *Franhueberia* makes direct comparison difficult. *Armoricaphyton* shows a comparatively small amount of secondary xylem compared with *Franhueberia*. Also, there is a difference in the anatomy of rays. *Armoricaphyton* exhibits comparatively few rays, which are diverse in form and size, whereas *Franhueberia* shows numerous rays and these are regularly distributed and consistent in form. The unnamed plant from New Brunswick (Gerrienne *et al*., 2011) differs from *Armoricaphyton* in the more oval-elongate form of both the protoxylem and primary xylem, but the most important feature that distinguishes this plant from *Armoricaphyton* is the occurrence of numerous rays. A sterome has not been reported in either *Franhueberia* or in the plant from New Brunswick. [See Hoffman & Tomescu (2013) for the table of comparisons with other Devonian plants that have evolved secondary vascular tissues.]

### Hydraulic properties

A total of 319 tracheid lumens were isolated and measured from a transverse section of axis imaged using PPC-SRμCT (Fig. 6 and Table 1). Measurements of tracheid element lumen area ranged greatly in size from 20 to 2600 $\mu m^2$, with a mean of 772 $\mu m^2$. The hydraulic diameters $D_H$ of these cells showed a mean value of 25.3 μm, with the largest values measuring up to 51.0 μm. The mean cell wall thickness was computed as 11.2 μm. This mean value is higher than the minimum value generally used for the study of hydraulic properties of extant plants, because it takes into account all the boundary points, including the points at the three or four cell intersections (Fig. 6). Nevertheless, the use of the mean value is justified in our study by the variability of the cell wall thickness around the different sides of the cell, which also show variable lengths. The total lumen area occupied an average of 58% of the total xylem area. The lumen specific hydraulic conductivity $k_s$ (Eqn. 6) was calculated as 17.4 $kg\ m^{-1}\ s^{-1}\ MPa^{-1}$. Sperry, Hacke & Wheeler (2005) found that the lumen resistivity is equal to the end wall resistivity (i.e. $k_{xylem} = k_{lumen}/2$, the sum of two conductances in series). According to this hypothesis, we can estimate that the total specific hydraulic conductivity of the xylem area is around 8.7 $kg\ m^{-1}\ s^{-1}$.

## DISCUSSION

Our analysis of the anatomy of *A. chateaupannense* indicates an affinity with Euphyllophytina (Kenrick & Crane, 1997a,b) based on the possession of centrarch primary xylem maturation, pseudomonopodial branching, a type of scalariform pitting and radially aligned xylem. We have not been able to identify the preserved remains of a cambium, which is probably a result of the insubstantial nature of this tissue and of the poor preservation of tissues surrounding the xylem. Nevertheless, the derivation of the wood from a cambium is strongly supported by the occurrence of rays and the evidence for both periclinal and anticlinal cell divisions within the xylem. The absence of secondary phloem might also be a preservational feature, but, in this case, might reflect true absence. There is evidence that secondary phloem was absent from many other early woody euphyllophytes, includ-

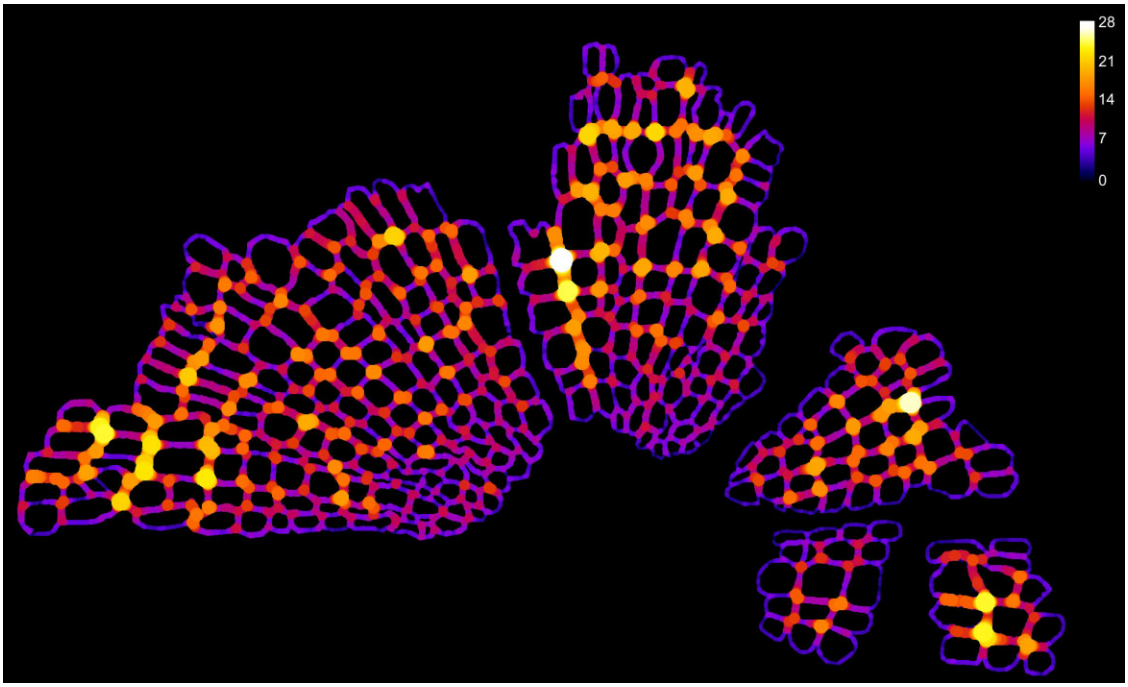


**Figure 6.** Transverse section of xylem cell lumens of *Armoricaphyton chateaupannense* extracted from the propagation phase contrast X-ray synchrotron microtomography (PPC-SRμCT) volume to map cell dimensions (CSD-07F-01). The geometrical parameters (i.e. area, diameter, perimeter) of each tracheid were measured to evaluate the individual hydraulic conductivity using the hydraulic radius approximation. The cell wall thickness was mapped using the Hildebrand algorithm in order to calculate the thickness-to-span ratio $(t/b)^2$, which reflects the sensitivity of the cells to transverse mechanical buckling under negative pressure. The brighter the colour, the thicker the double cell wall (μm scale).

**Table 1.** Mean value and standard deviation of main anatomical characteristics and hydraulic performance of *Armoricaphyton chateaupannense*. The specific conductivity $k_s$ was computed for the whole xylem area

| Lumen area/ xylem area (%) | Maximum diameter (μm) | Lumen area (μm²) | $D_H$ ($10^{-6}$ m) | $k_s$ (kg m$^{-1}$ s$^{-1}$ MPa$^{-1}$) | Mean cell wall thickness (μm) | Safety factor $(t/b)^2$ |
|---|---|---|---|---|---|---|
| 58 | 41.3 ± 12 | 772.8 ± 442 | 25.3 ± 8.66 | 17.4 | 11.2 | 0.037 ± 0.018 |

ing the sphenopsids and the cladoxylopsids (Niklas, 2000; Meyer-Berthaud *et al*., 2010). Cladoxylopsids are an extinct group of early forest shrubs and trees (Stein *et al*., 2007, 2012). Sphenopsids are thought to include living horsetails, but many early forms were also arborescent (Meyer-Berthaud *et al*., 2010). Secondary phloem was also absent from the arborescent lycopods (Niklas, 1997). These groups all possessed a unifacial cambium. Because we are unable to rule out the possibility that, in *A. chateaupannense*, the absence of secondary phloem is a result of poor preservation, we cannot currently define the cambium as unifacial or bifacial. Basal lignophytes, such as Archaeopteridales and Aneurophytales, and possibly also the fossil *Sphenophyllum* Brongniart (Eggert & Gaunt, 1973; Spicer & Groover, 2010), possessed a bifacial cambium that was capable of producing both secondary xylem and secondary phloem (Beck & Wight, 1988; Donoghue, 2005). Unlike most plants with a unifacial cambium, the xylem of *A. chateaupannense* shows clear evidence of anticlinal cell division. This implies that it could accommodate increasing girth through cell division. Anticlinal cell division of this sort is typical in the xylem of the lignophytes (Hilton & Bateman, 2006), and there is some evidence that it occurs in other euphyllophytes (e.g. cladoxylopsids) (Hilton, Geng & Kenrick, 2003; Meyer-Berthaud *et al*., 2004). The wood of *A. chateaupannense* exhibits a combination of features found in other early woody clades, and shows that these were present earlier in small-bodied plants by the Lower Devonian. These data show that the early evolution of

secondary xylem does not initially correlate with a significant increase in plant size (Gerrienne *et al*., 2011).

Our modelling of hydraulic performance in *A. chateaupannense* shows a high value for the specific hydraulic conductivity ($k_s$) that can be attributed to the numerous, large-diameter tracheids. These tracheids possess values of individual conductivity $k_i$ that are more typical of vessels in some extant angiosperms (Tyree & Zimmermann, 2002; Sperry, Hacke & Pittermann, 2006). Similar high conductivities were recently modelled for the tracheids of three Palaeozoic pteridosperms (*Lyginopteris* Potonié, *Medullosa* Cotta, *Callistophyton* Delevoryas & Morgan) by Wilson & Knoll (2010). Qualitatively, however, the hydraulic structure in *A. chateaupannense* more closely resembles extant gymnosperm early wood, except that the tracheids in the fossil, which differ in significant details of wall structure (P-type) from modern forms, have wider lumen areas and thinner cell walls. In *A. chateaupannense*, the mean cell thickness-to-span ratio $(t/b)^2$ was 0.0372. This value is low compared with that of extant tracheid-based trees (Hacke *et al*., 2001; Pittermann *et al*., 2006; Sperry, Hacke & Pittermann, 2006). For example, our value is comparable with that calculated (0.04) for *Taxodium distichum* (L.) Rich. (Pittermann *et al*., 2006). This species shows a similar $t/b$ value, which is the lowest found by Pittermann *et al*. (2006) for wood in stems. Hacke *et al*. (2001) proposed a general regression between the implosion safety factor and cavitation sensitivity, $P_{50}$, which represents the negative pressure required to generate a 50% loss of conductivity. An extrapolation of this regression would lead to $P_{50} = -1$ MPa for *A. chateaupannense*. We are cautious about drawing functional implications from these calculations, because there are insufficient environmental data to show to what extent the plant experienced water stress. This low value of $P_{50}$ indicates that the anatomical structure of this early land plant was probably not well adapted to withstand water stress-induced cavitation. All calculated hydraulic properties indicate that the anatomy of *A. chateaupannense* was suited to a high conductive performance associated with low mechanical resistance to hydraulic tension.

The hydraulic conductance of the xylem is also affected by the relative number, distribution and type of pitting in the tracheid cell wall. The modelling of this aspect of conductance in the earliest vascular plants is complicated by differences in cell wall structure from modern plants. Recently, Wilson & Fischer (2011) modelled the hydraulic resistance of the tracheid cell wall of the early fossil *Asteroxylon* Kidston & Lang which possessed G-type tracheids (Kenrick & Edwards, 1988; Kenrick & Crane, 1991; Edwards, 1993). They concluded that the xylem had a surprisingly high conductivity and a correspondingly low hydraulic safety. However, their simple scalariform pit model did not consider the effects of the presence of secondary wall material extending between annular bars, which would significantly restrict the effective porosity of the tracheid wall. Similarly, the estimation of the porosity of the scalariform pitting of the tracheids of *A. chateaupannense* is complicated because it possesses P-type tracheids (Fig. 6). Here, also extending over the pit apertures is an additional perforate sheet of secondary wall material. We have not attempted to model this, but we suggest that the effect of this sheet of secondary wall material in both G-type and P-type tracheids is to provide additional mechanical resistance to the cell wall. This could improve the mechanical behaviour of the stem and reduce the sensitivity of the tracheid to transverse buckling. A more complete quantification of hydraulic conductance in these early plants requires an accurate model of water flow between cells in G-type and P-type tracheids.

The early evolution of the plant vascular system has been widely discussed in the context of various environmental drivers (Pittermann, 2010), plant physiology and function (Sperry, 2003; Sperry *et al*., 2006) and plant biomechanics (Niklas, 1997, 2000; Wilson & Knoll, 2010). The vascular system in most plants plays two primary roles: hydraulic conductance of fluids and mechanical support of above-ground organ systems. To fulfil both for a particular set of environmental conditions entails compromise, and this is reflected in the diverse range of conducting systems found in nature (Niklas, 1997; Sperry, 2003; Pittermann, 2010). Some evolutionary trends appear to be clear. For example, measurements from fossil plants show that the maximum tracheid diameter in primary xylem and the maximum amount of xylem in a stem increased rapidly during the early evolution of wood through the Devonian (Niklas, 1985). From a biomechanical perspective, increasing the stem diameter through the addition of wood increases Young's modulus and therefore the rigidity of the stem (Speck, 1994; Niklas & Speck, 2001; Sperry, 2003; Sperry *et al*., 2006). Furthermore, wood can vary greatly in density and, for a given trunk diameter, higher density equates to greater strength (Niklas & Spatz, 2012). However, theory indicates that, in terms of construction cost, the most effective approach to increase stem diameter, and therefore overall rigidity, is through the addition of low-density wood (Anten & Schieving, 2010; Awad *et al*., 2012; Larjavaara & Muller-Landau, 2012). Our measurements of tracheid diameter and tracheid wall thickness to span ratio in *A. chateaupannense* indicate that wood of low density was the strategy adopted by the earliest woody plants.

## CONCLUSION

PPC-SRμCT is a useful tool for three-dimensional imaging of fossil woods permineralized in pyrite ($FeS_2$). The method is non-invasive and enables virtual dissection, facilitating the characterization and measurement at the submicrometre level.

Wood first evolved in small, leafless, rootless plants (euphyllophytes) in the lower part of the Devonian period, at *c*. 407 Ma. This early wood developed from a cambium that gave rise to secondary xylem and to rays. Cambium cells were capable of anticlinal divisions, which facilitated and accommodated increasing girth.

Hydraulic properties were calculated from measurements taken from the PPC-SRμCT images. The results indicate that the wood was suited to high conductive performance with low mechanical resistance to hydraulic tension. We argue that axis rigidity in the earliest woody plants evolved through the development of low-density woods.

## ACKNOWLEDGEMENTS

This work was performed as part of the PhD thesis of C.S.-D. under the supervision of D. G. Strullu (Université d'Angers, France) and P. Gerrienne (Université de Liège, Belgium). C.S.-D. would like to thank R. Jospin, Châteaupanne Quarry director, for allowing access and collection of fossil specimens. She thanks the members of the Laboratoire PPM, Université de Liège for their welcome during her visits and for technical assistance. M. F. Baslé and D. Chappard (Université d'Angers) are acknowledged for the use of the Scanning Electron Microscope and Faxitron X-ray system, and R. Mallet for technical assistance at the 'Service Commun d'Imageries et d'Analyses Microscopiques de l'Université d'Angers'. The European Synchrotron Radiation Facility (ESRF) and ID19 beamline are acknowledged for providing the necessary beam time for this experiment. The authors thank M. Ballèvre (Université de Rennes, France) and C. Ducassou (German University of Technology, Oman) for their useful comments. H. Taylor (Natural History Museum) is acknowledged for the photograph of the fossil plant preserved as a coaly compression (Fig. 2C). C.S.-D. received financial support from the European Commission under the Marie Curie Intra-European Fellowship Programme FP7-People-2011-SYMBIONTS.

## REFERENCES

**Anten NPR, Schieving F. 2010.** The role of wood mass density and mechanical constraints in the economy of tree architecture. *American Naturalist* **175:** 250–260.

**Awad H, Herbette S, Brunel N, Tixier A, Pilate G, Cochard H, Badel E. 2012.** No trade-off between hydraulic and mechanical properties in several transgenic poplars modified for lignins metabolism. *Environmental and Experimental Botany* **77:** 185–195.

**Banks HP, Leclercq S, Hueber FM. 1975.** Anatomy and morphology of *Psilophyton dawsonii*, sp. nov. from the late Lower Devonian of Quebec (Gaspé), and Ontario, Canada. *Palaeontographica Americana* **8:** 75–127.

**Beck CB, Wight DC. 1988.** Progymnosperms. In: Beck CB, ed. *Origin and evolution of gymnosperms*. New York: Columbia University Press, 57–61.

**Boyce CK. 2010.** The evolution of plant development in a paleontological context. *Current Opinion in Plant Biology* **13:** 102–107.

**Brodersen CR, Lee EF, Choat B, Jansen S, Phillips RJ, Shackel KA, McElrone AJ, Matthews MA. 2011.** Automated analysis of three-dimensional xylem networks using high-resolution computed tomography. *New Phytologist* **191:** 1168–1179.

**Collinson ME, Smith SY, van Konijnenburg-van Cittert JHA, Batten DJ, van der Burgh J, Barke J, Marone F. 2013.** New observations and synthesis of Paleogene heterosporous water ferns. *International Journal of Plants Sciences* **174:** 350–363.

**Collinson ME, Smith SY, Manchester SR, Wilde V, Howard LE, Robson B, Ford D, Marone F, Fife JL, Stampanoni M. 2012.** The value of x-ray approaches in the study of the Messel fruit and seed flora. *Palaeobiodiversity and Palaeoenvironments* **92:** 403–416.

**Dannenhoffer JM, Bonamo PM. 2003.** The wood of *Rellimia* from the Givetian of New York. *International Journal of Plant Sciences* **164:** 429–441.

**Devore ML, Kenrick P, Pigg KB, Ketcham RA. 2006.** Utility of high resolution x-ray computed tomography (HRXCT) for paleobotanical studies: an example using London Clay fruits and seeds. *American Journal of Botany* **93:** 1848–1851.

**Donoghue MJ. 2005.** Key innovations, convergence, and success: macroevolutionary lessons from plant phylogeny. *Paleobiology* **31:** 77–93.

**Doran JB. 1980.** A new species of *Psilophyton* from the Lower Devonian of northern New Brunswick, Canada. *Canadian Journal of Botany* **58:** 2241–2262.

**Edwards D. 1993.** Cells and tissues in the vegetative sporophytes of early land plants. *New Phytologist* **125:** 225–247.

**Edwards D. 2003.** Xylem in early tracheophytes. *Plant Cell and Environment* **26:** 57–72.

**Edwards D, Li CS, Raven JA. 2006.** Tracheids in an early vascular plant: a tale of two branches. *Botanical Journal of the Linnean Society* **150:** 115–130.

**Eggert DA, Gaunt DD. 1973.** Phloem of *Sphenophyllum*. *American Journal of Botany* **60:** 755–770.

**Feist M, Liu J, Tafforeau P. 2005.** New insights into Paleozoic charophyte morphology and phylogeny. *American Journal of Botany* **92:** 1152–1160.

**Friis EM, Crane P, Pedersen KR, Bengston S, Donoghue PCJ, Grimm GW, Stampanoni M. 2007.** Phase-contrast

x-ray microtomography links Cretaceous seeds with Gnetales and Benettitales. *Nature* **450:** 549–552.

**Friis EM, Pedersen KR, Endress PK. 2013.** Floral structure of extant *Quintinia* (Paracryphiales, campanulids) compared with the Late Cretaceous *Silvianthemum* and *Bertilanthus*. *International Journal of Plant Sciences* **174:** 647–664.

**Gee CT. 2013.** Applying microCT and 3D visualization to Jurassic silicified conifer seed cones: a virtual advantage over thin-sectioning. *Applications in Plant Sciences* **1:** 1300039.

**Gerrienne P. 1997.** The fossil plants from the Lower Devonian of Marchin (northern margin of Dinant Synclinorium, Belgium). V. *Psilophyton genselia* sp. nov. with hypotheses on the origin of Trimerophytina. *Review of Palaeobotany and Palynology* **98:** 303–324.

**Gerrienne P, Gensel P, Strullu-Derrien C, Lardeux H, Steemans P, Prestiani C. 2011.** A simple type of wood in two Early Devonian plants. *Science* **333:** 837.

**Hacke UG, Sperry JS, Pockman WT, Davis SD, McCulloch KA. 2001.** Trends in wood density and structure are linked to prevention of xylem implosion by negative pressure. *Oecologia* **126:** 457–461.

**Hartman CM, Banks HP. 1980.** Pitting in *Psilophyton dawsonii*, an early Devonian trimerophyte. *American Journal of Botany* **67:** 400–412.

**Hildebrand T, Rüegsegger P. 1996.** A new method for the model-independent assessment of thickness in three-dimensional images. *Journal of Microscopy* **185:** 67–75.

**Hilton J, Bateman RM. 2006.** Pteridosperms are the backbone of seed-plant phylogeny. *Journal of the Torrey Botanical Society* **133:** 119–168.

**Hilton J, Geng B, Kenrick P. 2003.** A novel Late Devonian (Frasnian) woody cladoxylopsid from China. *International Journal of Plant Sciences* **164:** 793–805.

**Hoffman LA, Tomescu MF. 2013.** An early origin of secondary growth: *Franhueberia gerriennei* gen. et sp. nov. from the Lower Devonian of Gaspé (Quebec, Canada). *American Journal of Botany* **100:** 754–763.

**Jones TP, Rowe N. 1999.** Embedding techniques, adhesives and resins. In: Jones TP, Rowe RP, eds. *Fossil plants and spores: modern techniques*. Geological Society of London. Cambridge: Cambridge University Press, 71–75.

**Kenrick P. 1999.** Opaque petrifaction techniques. In: Jones TP, Rowe RP, eds. *Fossil plants and spores. Modern techniques*. Geological Society of London. Cambridge: Cambridge University Press, 87–91.

**Kenrick P, Crane PR. 1991.** Water-conducting cells in early fossil land plants: implications for the early evolution of tracheophytes. *Botanical Gazette* **152:** 335–336.

**Kenrick P, Crane PR. 1997a.** *The origin and early diversification of land plants: a cladistic study*. Washington & London: Smithsonian Institution Press.

**Kenrick P, Crane PR. 1997b.** The origin and early evolution of plants on land. *Nature* **389:** 33–39.

**Kenrick P, Edwards D. 1988.** The anatomy of Lower Devonian *Gosslingia breconensis* Heard based on pyritized axes, with some comments on the permineralization process. *Botanical Journal of the Linnean Society* **97:** 95–123.

**Lachaud S, Catesson AM, Bonnemain JL. 1999.** Structure and functions of the vascular cambium. *Comptes Rendus de l'Académie des Sciences, Paris* **322:** 633–650.

**Lak M, Néraudeau D, Nel A, Cloetens P, Perrichot V, Tafforeau P. 2008.** Phase contrast x-ray synchrotron imaging: opening access to fossil inclusions in opaque amber. *Microscopy and Microanalysis* **14:** 251–259.

**Larjavaara M, Muller-Landau HC. 2012.** Still rethinking the value of high wood density. *American Journal of Botany* **99:** 165–168.

**Mannes D, Marone F, Lehmann E, Stampanoni M, Niemz P. 2010.** Application areas of synchrotron radiation tomographic microscopy for wood research. *Wood Science and Technology* **44:** 67–84.

**Meyer-Berthaud B, Rücklin M, Soria A, Belka Z, Lardeux H. 2004.** Frasnian plants from the Dra Valley, southern Anti-Atlas, Morocco. *Geological Magazine* **6:** 675–686.

**Meyer-Berthaud B, Soria A, Decombeix AL. 2010.** The land plant cover in the Devonian: a reassessment of the evolution of the tree habit. *Geological Society London, Special Publications* **339:** 59–70.

**Morzadec P, Paris F, Plusquellec Y, Racheboeuf P, Weyant M. 1988.** Devonian stratigraphy and paleogeography of the Armorican Massif (Western France). In: McMillan NJ, Embry AF, Glass DJ, eds. *Devonian of the world, Vol. 1*. Calgary: Canadian Society of Petroleum Geologists, 401–420.

**Niklas KJ. 1985.** The evolution of tracheid diameter in early vascular plants and its implications on the hydraulic conductance of the primary xylem strand. *Evolution* **39:** 1110–1122.

**Niklas KJ. 1997.** *The evolutionary biology of plants*. Chicago, IL: University of Chicago Press.

**Niklas KJ. 2000.** The evolution of plant body plans – a biomechanical perspective. *Annals of Botany* **85:** 411–438.

**Niklas KJ, Spatz HC. 2012.** Mechanical properties of wood disproportionately increase with increasing density. *American Journal of Botany* **99:** 169–170.

**Niklas KJ, Speck T. 2001.** Evolutionary trends in safety factors against wind-induced stem failure. *American Journal of Botany* **88:** 1266–1278.

**Pallardy SG. 2008.** *Physiology of woody plants*, 3rd edn. San Diego, CA: Academic Press.

**Pittermann J. 2010.** The evolution of water transport in plants: an integrated approach. *Geobiology* **8:** 112–139.

**Pittermann J, Sperry JS, Wheeler JK, Hacke UG, Sikkema EH. 2006.** Mechanical reinforcement of tracheids compromises the hydraulic efficiency of conifer xylem. *Plant Cell and Environment* **29:** 1618–1628.

**Rasband WS. 2012.** *Image J*. Bethesda, MD: US National Institutes of Health, 1997–2014. Available at: http://imagej.nih.gov/ij/

**Scotese CR. 2001.** *Digital paleogeographic map archive on CD-ROM*. Arlington, TX: PALEOMAP Project.

**Sisavath S, Jing X, Zimmerman R. 2001.** Laminar flow through irregularly-shaped pores in sedimentary rocks. *Transport in Porous Media* **45:** 41–62.

**Smith SY, Collinson ME, Simpson DA, Rudall PJ, Marone F, Stampanoni M. 2009.** Elucidating the affinities and habitat of ancient, widespread Cyperaceae: *Volkeria messelensis* gen. et sp. nov., a fossil mapanioid sedge from the Eocene of Europe. *American Journal of Botany* **96:** 1506–1518.

**Speck T. 1994.** Bending stability of plant stems: ontogenetical, ecological and phylogenetical aspects. *Biomimetics* **2:** 109–128.

**Sperry JS. 2003.** Evolution of water transport and xylem structure. *International Journal of Plant Sciences* **164:** S115–S127.

**Sperry JS, Hacke UG, Pittermann J. 2006.** Size and function in conifer tracheids and angiosperm vessels. *American Journal of Botany* **93:** 1490–1500.

**Sperry JS, Hacke UG, Wheeler JK. 2005.** Comparative analysis of end wall resistivity in xylem conduits. *Plant, Cell & Environment* **28:** 456–465.

**Spicer R, Groover A. 2010.** Evolution of development of vascular cambia and secondary growth. *New Phytologist* **186:** 577–592.

**Stein WE, Berry CM, VanAller Hernick L, Mannolini F. 2012.** Surprisingly complex community discovered in the mid-Devonian fossil forest at Gilboa. *Nature* **483:** 78–81.

**Stein WE, Mannolini F, VanAller Hernick L, Landing E, Berry CM. 2007.** Giant cladoxylopsid trees resolve the enigma of the Earth's earliest forest stumps at Gilboa. *Nature* **446:** 904–907.

**Strullu-Derrien C. 2010.** Recherches sur la colonisation du milieu terrestre par les plantes au cours du Dévonien inférieur et sur les interactions plantes/microorganismes durant les périodes Dévonien-Carbonifère. DPhil Thesis, Angers University. Available at: http://www.sudoc.fr/157448290.

**Strullu-Derrien C, Ducassou C, Ballèvre M, Dabard MP, Gerrienne P, Lardeux H, Le Hérissé A, Robin C, Steemans P, Strullu DG. 2010.** The early land plants from the Armorican Massif: sedimentological and palynological considerations on age and environment. *Geological Magazine* **147:** 830–843.

**Tafforeau P, Smith TM. 2008.** Nondestructive imaging of hominoid dental microstructure using phase contrast x-ray synchrotron microtomography. *Journal of Human Evolution* **54:** 272–278.

**Tyree MT, Zimmermann MH. 2002.** *Xylem structure and ascent of sap*, 2nd edn. Springer Series in Wood Science. Berlin & New York: Springer-Verlag.

**Wilson JP, Fischer WW. 2011.** Hydraulics of *Asteroxylon mackei*, an early Devonian vascular plant, and the early evolution of water transport tissue in terrestrial plants. *Geobiology* **9:** 121–130.

**Wilson JP, Knoll AH. 2010.** A physiologically explicit morphospace for tracheid-based water transport in modern and extinct seed plants. *Paleobiology* **36:** 335–355.